J. Zool., Lond. (1982) **197**, 483–495

Structure and function in the tail of the Pumpkinseed sunfish (*Lepomis gibbosus*)

GEORGE V. LAUDER
Department of Anatomy, University of Chicago, Chicago, IL 60637, U.S.A.

(Accepted 8 December 1981)

(With 1 plate and 7 figures in the text)

Patterns of *in vivo* bone deformation in the caudal skeleton of sunfishes have been studied with rosette strain gauges. An anatomical description of caudal osteology and myology is provided for comparison with other actinopterygian fishes and as an aid in interpreting the bone strain patterns. Peak bone strain during fast-start acceleration was −3213 με and the peak strain rate was -296×10^3 με/s. During steady locomotion, strain rates and magnitudes were considerably lower ($10–85 \times 10^3$ με/s and 379–1074 με, respectively). The main strain peak during fast-starts occurs during kinematic stage one. Mean principal tensile and compressive angles are aligned parallel and perpendicular to the body axis during fast-starts, while steady locomotion results in strain axes inclined at a mean angle of −34° to the body axis. These results are compared to strain data from other vertebrates: vertebrate bone is only very rarely subjected to deformations greater than 3100 με and to strain rates greater than 100×10^3 με/s. The role of this type of functional analysis in studying actinopterygian locomotor patterns is discussed.

Contents

Introduction

The analysis of the process of locomotion in actinopterygian (ray-finned) fishes has received a considerable stimulus in the last ten years as a result of both theoretical hydrodynamic analyses of locomotor mechanics (e.g. Wu, 1971; Weihs, 1972, 1973; Lighthill, 1975), and experimental investigations of locomotor performance and mechanics (see especially Webb, 1975; Hoar & Randall, 1978). These analyses have provided important insights into the relationship between body form and locomotor performance (Gero, 1952; Bainbridge, 1958, 1963; Fierstine & Walters, 1968) and patterns of fin movement during hovering (Blake, 1979) and acceleration.

There are no data, however, on the patterns of internal structural deformations resulting from forces exerted by the fish on the external medium. Investigations demonstrating a

0022-5460/82/080483+13 $03.00/0

relationship between internal organizational features such as the structure of the caudal or axial skeleton and musculature, and externally imposed loads and whole-body deformations would be especially valuable in light of the important structural changes that have taken place in actinopterygian evolution. Major patterns of evolutionary change in the axial skeleton and caudal skeleton have been identified (e.g. alignment and fusion of the neural and haemal spines with the vertebral centra (Schaeffer, 1967; Lauder, 1980); modification of the primitive external caudal fin asymmetry into an externally symmetrical tail; structural changes in the support of caudal fin rays (see Patterson, 1968*a*, *b*, 1973; Patterson & Rosen, 1977), but we still have little or no idea of the functional correlates of these changes. Does, for example, the structure of the tail in *Amia* produce different patterns of stress and strain on the axial skeleton than the tail of *Salmo*, and are such patterns primitive for ray-finned fishes?

In this paper an analysis of the *in vivo* pattern of bone deformation in the caudal fin of a centrarchid sunfish, *Lepomis gibbosus*, during both continuous locomotion and fast-start acceleration is provided. The study is intended to give an anatomical and experimental baseline for future work on structure/function relationships in fish locomotion, and for the interpretation and discovery of functional patterns in the evolution of actinopterygian locomotor systems.

Materials and methods

Strain gauge implantations and recordings were performed on four individuals of *Lepomis gibbosus* following the procedure described previously (Lauder & Lanyon, 1980). Rosette strain gauges (TML FRA-2, Techni Measure, U.K.) which consisted of three 120 ohm foil single-element gauges mounted at 45° angles to each other on a thin plastic base, were bonded to hypural 4 (see Plate 1). Hypural 4 was the only caudal element large enough to accommodate the gauges. The bonding agent was isobutyl 2-cyanoacrylate monomer. Bone strain was recorded with a three channel Vishay Strain Gauge Conditioner and a Honeywell 5600 tape recorder. Strain recordings were made at 37·5 cm/s and played back at 4·7 cm/s to preserve the frequency response of the strain signal. A Gould 260 chart recorder was used for final display of the recordings. Calibration of the gauges was permitted by known resistance changes provided by the Vishay strain gauge conditioner, and strain ($\Delta l/l$), a dimensionless parameter, was measured in microstrain (με), which is strain $\times 10^{-6}$. During implantation, care was taken to ensure that the strain gauge did not extend across several hypural bones. Rosette gauges allow the calculation of principal strain angle and thus a more accurate inference of loading situation than is possible using single element gauges. (For methods of calculating principal strain angles see Lanyon, 1976). The lateral musculature covering hypural 4 was reflected during gauge implantation and left intact to the extent possible. Following recording sessions, a radiograph was taken to ascertain the exact placement of the strain gauge and to permit orientation of the strain angle relative to bony landmarks. Strain patterns around the resting baseline value (which was taken as zero strain), visual observations of caudal fin motion and fin erection during fast-start accelerations were taken as evidence that major behavioural changes had not occurred as a result of gauge implantation.

Although the rosette gauges were large with respect to the area of hypural 4, the gauge and adhesive layer of glue were thin in comparison to the thickness of the hypural. Any increase in stiffness due to gauge adhesion would tend to reduce the peak strain values, and the maximum principal strain magnitudes reported here may thus be an underestimate. Experiments were performed at a water temperature of 20°C.

Anatomical descriptions were based on cleared and stained and dissected specimens of both *Lepomis macrochirus* and *L. gibbosus*. Illustrations were prepared with a Wild M5 dissecting stereomicroscope and camera lucida.

Results

Anatomy

A brief description of the osteology and myology of the caudal fin is presented as an aid in interpreting the subsequent functional analysis and for comparison with previous studies of caudal structure (Nursall, 1963; Nag, 1967; Cowan, 1969; Videler, 1975, 1977). Nomenclature of caudal musculature follows Winterbottom (1974).

Osteology

The caudal skeleton in *Lepomis gibbosus* and *L. macrochirus* is similar to that of many other acanthopterygian teleosts (see Patterson, 1968*b*; Rosen, 1973). Three epurals are usually present (Fig. 1). *Lepomis macrochirus* frequently only has two epurals as a result of fusion between epurals 2 and 3. Two uroneurals are present and the second uroneural is often firmly attached to the dorsal edge of hypural 5. Uroneural 1 and hypurals 4 and 5 are tightly attached to the ural complex (PU1 and U1), while hypurals 1 and 2 show some mobility relative to the ural complex (Fig. 1).

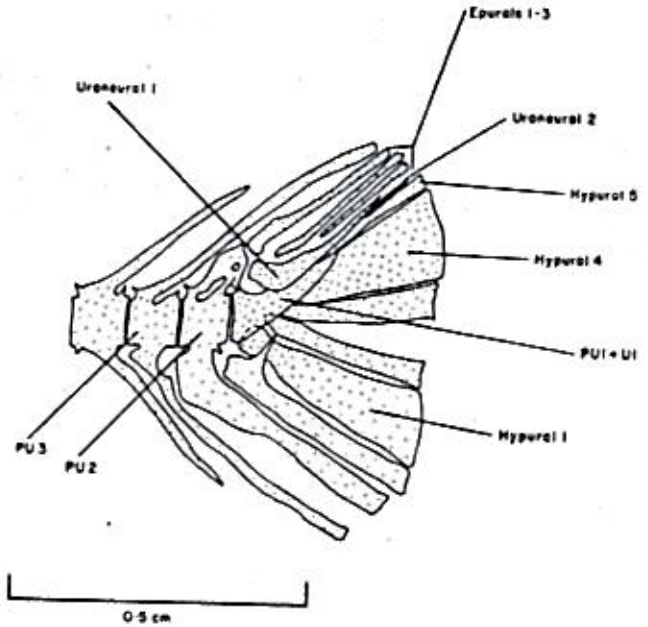

FIG. 1. Caudal skeleton of *Lepomis gibbosus*. The rosette strain gauges used to record hypural deformation were attached to hypural four. U_1, ural centrum one; PU_{1-3}, preural centra 1–3.

Myology

Lateralis superficialis (Figs 2, 3). In lateral view this muscle forms the dominant muscle of the caudal region. The dorsal and ventral borders of this muscle are not clearly separable and merge into the epaxial and hypaxial musculature. A mid-line superficial horizontal septum divides the lateralis superficialis into dorsal and ventral halves. Medially, the lateralis is clearly separate from the underlying hypochordalis and hypaxial musculature. The ventral half of the lateralis inserts posteriorly onto the head of rays 10–16, while the dorsal half slips medial to the hypochordal longitudinalis (Fig. 3) to insert on the head of rays 2–9.

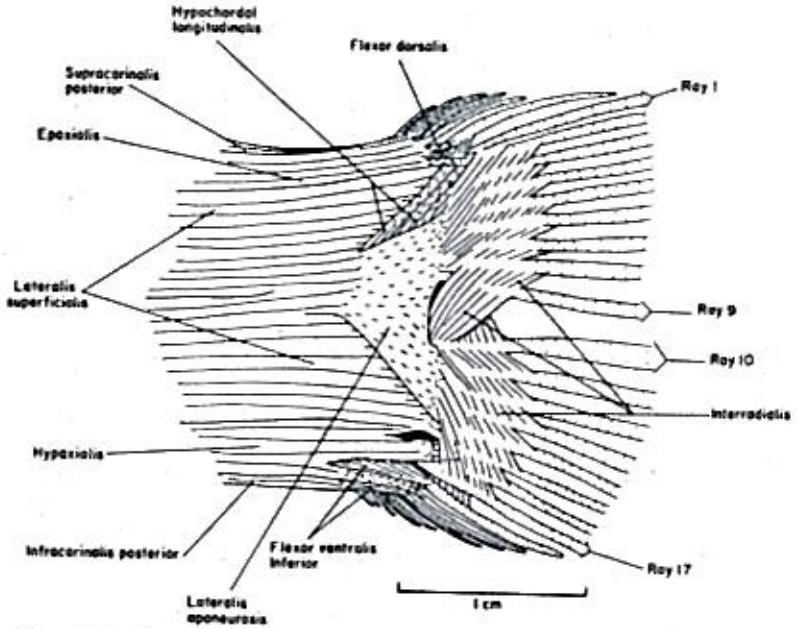

FIG. 2. Lateral view of the superficial layer of the caudal musculature in *Lepomis macrochirus*. The anterior procurrent dorsal caudal rays have been removed in this Figure and in Figs 3 and 4.

There is a broad *lateralis aponeurosis* which arises from the lateralis fibres near the midline (Fig. 2). This aponeurosis is clearly separate from and lies lateral to the underlying lateralis and hypochordalis muscle fibres. Some dorsal fibres of the lateralis superficialis have a broad insertion along the anterodorsal edge of the aponeurosis (Fig. 2). Ventrally the aponeurosis inserts into the heads of rays 10–14 while dorsally it inserts onto rays 4–9.

Hypaxialis. Posteriorly, the hypaxialis inserts via a short flat tendon onto the head of rays 15 and 16 (Fig. 2) and a second ventral tendon inserts on the two most posterior procurrent ventral caudal rays. This tendon lies just superficial to the flexor ventralis inferior. Medially,

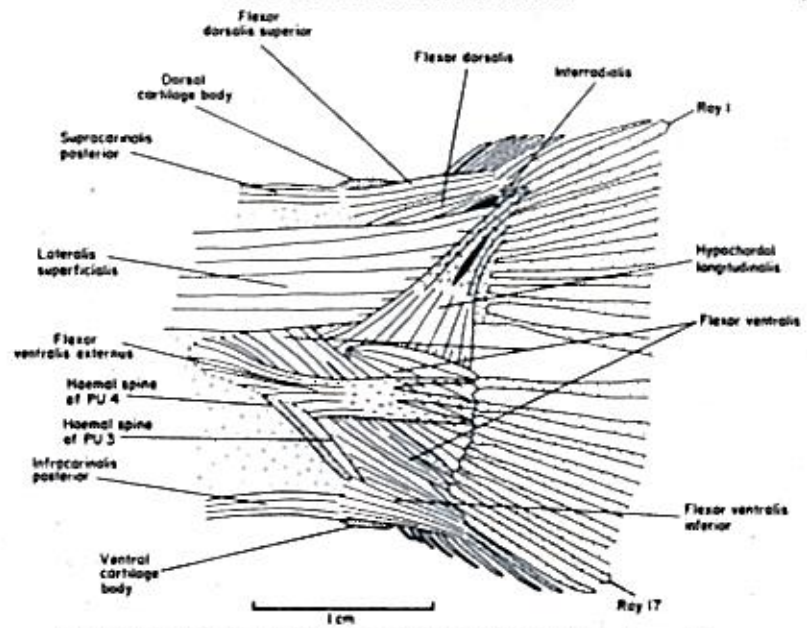

FIG. 3. Lateral view of the middle and deep caudal muscle layers in *Lepomis macrochirus*.

the hypaxial fibres in the caudal peduncle arise from both the haemal spines and from the lateral face of the sagittal septum connecting adjacent haemal spines.

Epaxialis. The epaxialis has a short tendinous insertion on the head of ray 2 (Fig. 2) and a dorsal insertion on the three most posterior procurrent rays.

Carinal muscles. The *infracarinalis posterior* (Figs 2, 3) inserts on the ventral cartilage body just anterior to the haemal spine of PU3. The *supracarinalis posterior* inserts on the dorsal cartilage body dorsal to the neural spine on preural vertebra number three (Fig. 3). The origin of these muscles is from the most posterior anal and dorsal fin pterygiophores, respectively (Winterbottom, 1974).

Interradialis (Fig. 2). The dorsal interradialis muscles extend anteroventrally between adjacent rays. Posteriorly the fibres connect only adjacent rays but anteriorly the superficial fibres extend between two or occasionally three rays. A small separate section of the dorsal interradialis connects hypural 5 to the most posterior dorsal procurrent ray (Fig. 2). The ventral interradialis muscles extend posteroventrally (i.e. at a 90° angle to the dorsal fibres) to connect adjacent fin rays. The anterior fibres cross several rays. Between rays 9 and 10, the dorsal inter-radialis overlies the ventral muscle fibres. A few fibres connect ray 17 with the most posterior procurrent ventral ray.

Hypochordal longitudinalis (Figs 3, 4). This muscle has a broad origin from the lateral surface of hypural 1, the parhypural, the spinous process of the parhypural, hypural 2 and the ural complex. Four distinct tendons insert on rays 1–4.

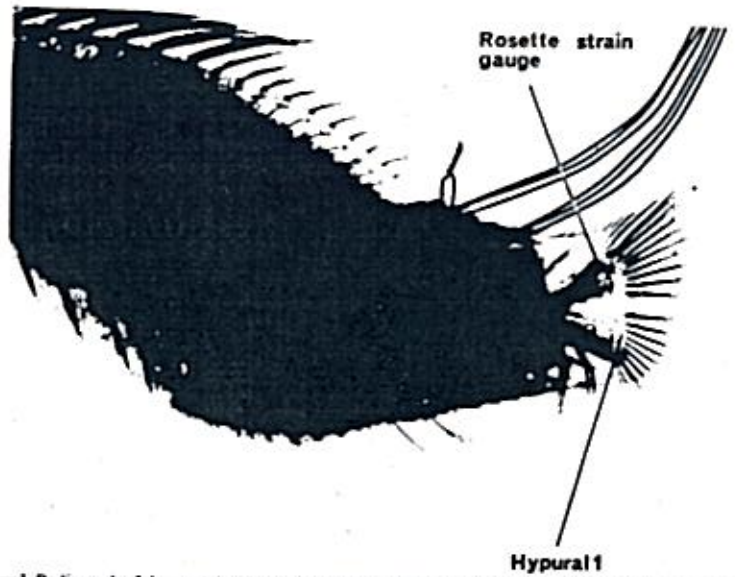

PLATE I. Radiograph of the caudal peduncle in *Lepomis gibbosus* to show the position of the rosette strain gauge used during one experiment. The fine wires lead from the rosette gauge to a small epoxy block loosely attached to the epaxial musculature by a loop of wire. Longer wires lead from this epoxy block to the strain gauge signal conditioner.

Flexor ventralis externus (Fig. 3). This muscle arises musculously from the lateral surface of preural vertebrae 3 and 4, the haemal spines of preural vertebrae 2 and 3, and the interspinous septum. The flexor ventralis externus extends posteriorly and thins out into a flat tendinous sheet inserting via separate tendons on rays 10, 11 and 12. Ventrally the tendon becomes very thin and merges with the fascia overlying the flexor ventralis.

Flexor ventralis (Fig. 3). This large muscle is divided into dorsal and ventral sections. The ventral section originates from preural vertebra 2 and the haemal spines of preural vertebrae 2 and 3. Insertion is on rays 16 and 17 only. The dorsal section originates from the lateral surface of preural vertebrae 2 and 3, the ural complex, and the dorsally projecting spine on the parhypural, and from the lateral surface of hypural 1 and the parhypural. The dorsal section inserts on rays 10–16.

Flexor ventralis inferior. The origin of this muscle is from the anterior surface of the anteroventral cartilage body, the median septum between the haemal spines of preural vertebrae 2 and 3, and the haemal spine of preural vertebra 3. Insertion is on the four most posterior ventral procurrent fin rays.

Flexor dorsalis (Figs 3, 4). The flexor dorsalis has a broad origin from the dorsal surface of preural vertebrae 2, 3 and 4, from the neural spines and interspinous septa of preural vertebrae 2 and 3, the ural complex, uroneurals, and epurals 2 and 3, but not from hypurals 3 and 4. The flexor dorsalis inserts on rays 1–9.

Flexor dorsalis superior (Fig. 3). The ventral border of this muscle is not distinct from the flexor dorsalis. The flexor dorsalis superior arises from epurals 1–3 and inserts on the three or four most posterior dorsal procurrent caudal fin rays.

Hypural strain patterns

Hypural strain patterns were analysed for both fast-start accelerations and for slow, continuous (steady) locomotion. (See Plate I for strain gauge location.) During fast-starts, peak

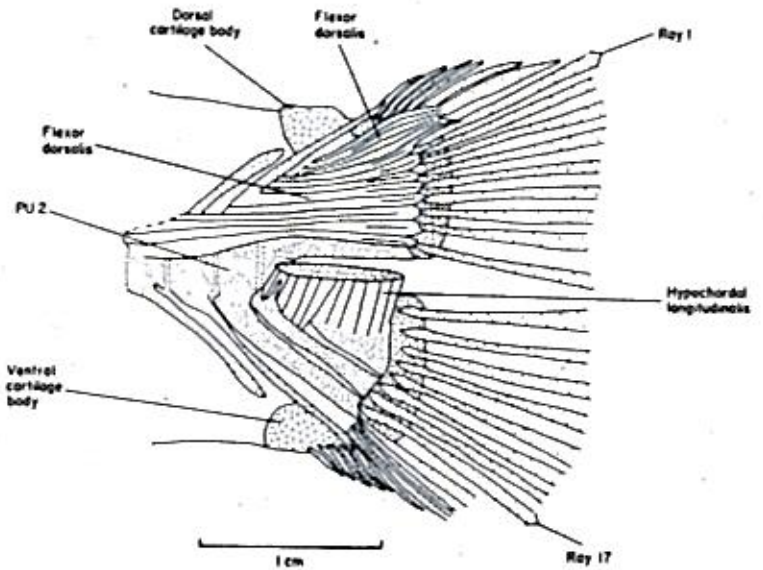

FIG. 4. Lateral view of the flexor dorsalis and origin of the hypochordal longitudinalis in *Lepomis macrochirus*.

principal tensile and compressive strains were reached within 20 ms (Figs 5(a) and 6). The peak principal strains recorded were $-3213\ \mu\varepsilon$ and $2764\ \mu\varepsilon$ and the peak (imposed) principal strain rate was $-296\times10^3\ \mu\varepsilon/s$. Most fast-starts showed strain rates over $-200\times10^3\ \mu\varepsilon/s$ but the mean principal strains were $1026\ \mu\varepsilon$ and $-1906\ \mu\varepsilon$, a ratio of nearly one to two. Principal strain orientation on the hypural during the fast-start remained relatively constant after an initial change (Fig. 6). Orientation of the principal strains at peak strain magnitude varied relatively little between fast-starts. The total range of variation was 13° and the principal compressive strain was parallel to the horizontal body axis (Fig. 7: FS). The greater the compressive strain magnitude, however, the greater the anteroventral tilt in the axis of peak principal compressive strain.

During continuous locomotion hypural strain oscillated around the resting value as the tail was swept from side to side (Fig. 5(b)). Ipsilateral strain peaks are defined here as those

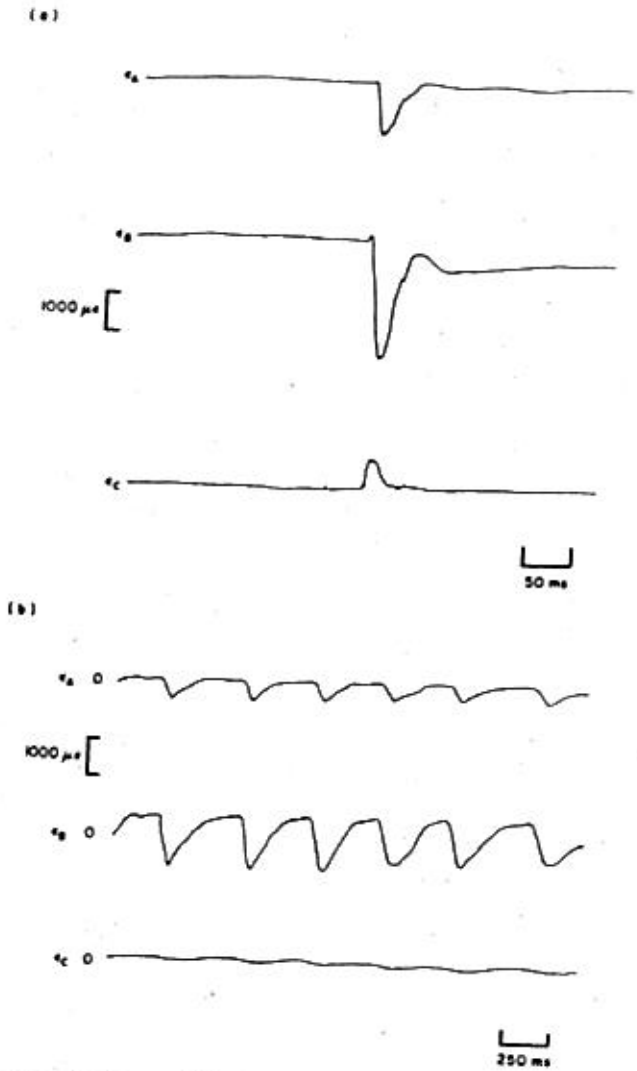

FIG. 5. (a). Pattern of bone strain recorded from hypural 4 during a contralateral fast-start (see text). The three traces represent output from each of the single-element components of the rosette gauges (axes ε_A, ε_B, ε_C; see Lanyon, 1976). (b) Pattern of bone strain during steady swimming. Zero line indicates resting strain level. Note the different magnitudes and rates of strain as compared to fast-starts.

occurring as the caudal fin is swept towards the side of the tail bearing the strain gauge, while contralateral peaks are those occurring as the tail moved away from the side with the strain gauge. The angles and relative magnitudes of principal strain during continuous locomotion are shown in Fig. 7. Note the close correspondence in angle between ipsilateral and contralateral peaks (no significant difference in angle was found). Mean principal strains for contralateral peaks were $-1074\ \mu\varepsilon$ and $574\ \mu\varepsilon$, while ipsilateral peaks were $-379\ \mu\varepsilon$ and $729\ \mu\varepsilon$. Ipsilateral peaks were thus lower than contralateral values probably because of partial disruption of the overlying musculature during strain gauge implantation. The ratio of mean maximum principal compressive to tensile strain was different for contralateral (−1·8) and ipsilateral (−0·51) caudal fin movements.

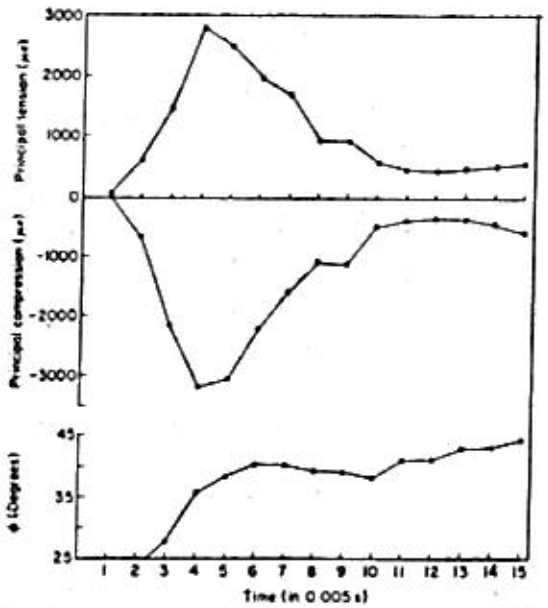

FIG. 6. Principal tensile and compressive strains and strain angle (φ) calculated for a fast-start.

Maximum imposed strain rates (measured over a 10 ms interval) varied from $85\times10^3\ \mu\varepsilon/s$ to $10\times10^3\ \mu\varepsilon/s$ during slow locomotion. The mean strain rate (calculated from principal strains) was $28\times10^3\ \mu\varepsilon/s$. Strain orientation on the hypural during steady swimming was consistently different from that during fast-starts (Fig. 7: CLC, CLI). The mean principal compressive or tensile strain orientation relative to the body axis (depending on whether ipsilateral or contralateral maxima are considered) was −34°, significantly different from the 0° mean for fast-starts (Fig. 7).

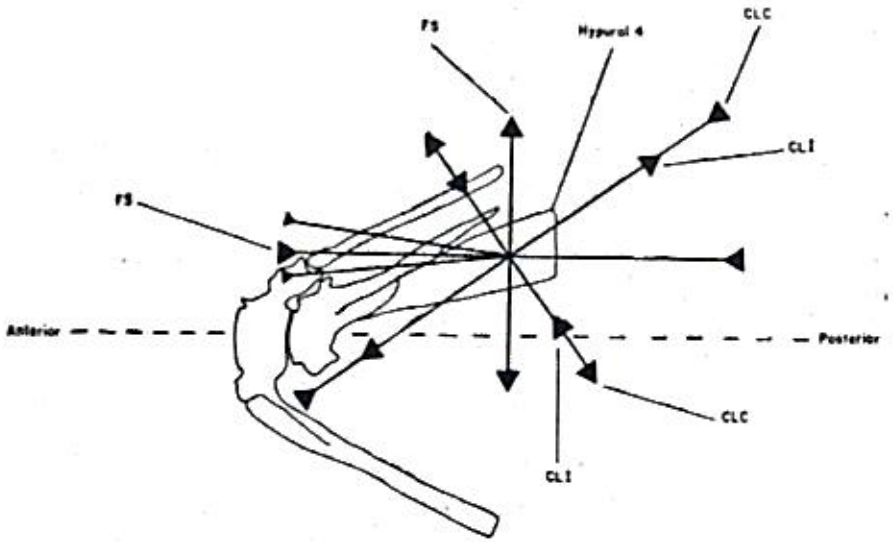

FIG. 7. Orientation of the principal compressive and tensile strains on hypural 4 in *Lepomis gibbosus*. FS: fast-starts; the two compressive axes on either side of the principal horizontal fast start axis indicate the range of variation around the mean. CLC: continuous locomotion, contralateral peaks (see text). CLI: continuous locomotion, ipsilateral peaks. The lengths of the axes indicate the relative magnitudes of tensile (⟵●⟶) and compressive (●⟶⟵●) strains for each category.

Discussion

Caudal osteology and myology in *Lepomis gibbosus* and *macrochirus* shows many similarities to caudal structure in other perciform fishes (see Nag, 1967; Cowan, 1969; Winterbottom, 1974). The presence of a hypochordal longitudinalis and dorsal and ventral flexors is a general teleost (or possibly halecostome) condition. *Polypterus* appears to lack both a hypochordal longitudinalis and interradialis muscles (Nursall, 1963). No adductor dorsalis muscle was found in *Lepomis*.

Videler (1975) has studied the function of several caudal muscles in relation to tail movements in *Tilapia*. He demonstrated by electromyography that there is extensive overlap in activity periods of the lateralis superficialis, the flexor ventralis, flexor dorsalis, and hypochordal longitudinalis during steady swimming. Videler also showed that the flexor dorsalis superior and flexor ventralis inferior are active during both ipsilateral and contralateral tail strokes to abduct the fin rays. While no electromyographic studies have been conducted of fast-start performance, Webb (1977, 1978) and Eaton *et al.* (1977) have shown that median and caudal fin erection occurs just prior to rapid acceleration. The degree of caudal fin abduction and electrical activity in caudal muscles will have an important influence on the strain pattern experienced by the hypurals. Asymmetrical activity between the dorsal and

ventral caudal muscles (particularly the flexor dorsalis and ventralis, flexor dorsalis superior and inferior) could easily account for the change in angle of hypural strain (Fig. 7) between fast-starts and steady locomotion. Unfortunately, no work is available on the electromyographic activity of caudal musculature in relation to tail kinematics during the fast-start.

The strain patterns recorded on hypural 4 during fast-start performance (Fig. 7: FS) are consistent with a loading regime of lateral bending in the horizontal plane. Principal tensile strains are oriented exactly perpendicular to the body axis, parallel to the axis of bending. The rapid and consistent rise to maximum strain during the early phase of the fast-start (Fig. 5(a)) appears to occur during kinematic stage one of the fast-start as defined in Webb (1977, 1978). This stage lasts about 45 ms (kinematic data for *Lepomis* are presented in Webb, 1978) and is followed by a less stereotyped kinematic stage two, the main propulsive stroke (Weihs, 1973; Webb, 1978: 215). Secondary modulations of hypural bone strain following the rapid initial rise appear to correspond to kinematic stage two which, at 15°C, lasts an average of 87 ms in *Lepomis* (Webb, 1978: fig. 3). Subsequent strain patterns during the variable kinematic stage three were of considerably less magnitude than those of stages one and two and approached values seen in steady swimming.

The strain patterns recorded during continuous locomotion differed significantly from the fast-start pattern (Fig. 7). The observed strain orientations and magnitudes for steady swimming are consistent either with a loading regime of hypural bending around an oblique axis parallel to the more vertical tensile and compressive strains in Fig. 7, or with a twisting moment. If, as the hypural is moved laterally through the water, a force is applied to the posterodorsal aspect of the hypural in a direction opposite to the direction of tail movement, then the hypural would tend to rotate about its attachment to the ural complex. This rotation would result in the oblique orientation of the principal strain axes observed in steady swimming. Because a strain gauge could not be simultaneously implanted on the contralateral side without excessive disruption of muscle function, the pure bending and bending plus twisting loading regimes could not be distinguished (see Lanyon, 1973, 1976; Hylander, 1979; Lauder & Lanyon, 1980, for more general discussions of the inference of bending and twisting loads from strain data). The difference in strain pattern between fast-starts and steady swimming may be due either to the different mechanical situations experienced by the tail during these two locomotor patterns, different patterns of caudal muscle activity, or both. Only detailed simultaneous study of muscle activity, kinematics and bone strain will allow the basis for the different strain patterns to be understood.

The strain rates and magnitudes recorded during steady swimming accord well with values obtained in other vertebrates (regardless of size). For example, rosette strain gauges on the femur of *Varanus* revealed peak strain magnitudes of $-850\,\mu\varepsilon$ and peak strain rates of $12\times10^3\,\mu\varepsilon/s$ (Lanyon, Lauder & Rubin, unpublished data). Comparable data on other vertebrates include: *Ovis* locomotion—peak strain $1637\,\mu\varepsilon$, peak strain rate $42\times10^3\,\mu\varepsilon/s$; *Anser* flying—$-2700\,\mu\varepsilon$, $36\times10^3\,\mu\varepsilon/s$ (Lanyon, unpublished); *Equus* locomotion—$3200\,\mu\varepsilon$, $-76\times10^3\,\mu\varepsilon/s$ (Lanyon & Rubin, 1980); *Rattus* locomotion—$500\,\mu\varepsilon$, $17\times10^3\,\mu\varepsilon/s$ (A. Biewener, unpublished). During fast-starts, however, the strain magnitudes reported here in *Lepomis* ($-3213\,\mu\varepsilon$) equal the peak reported previously for vertebrate locomotion (Lanyon & Rubin, 1980) and the peak strain rate of $-296\times10^3\,\mu\varepsilon/s$ exceeds all reports for locomotor performance. Only strain rates recorded on the sunfish operculum during feeding (Lauder & Lanyon, 1980) exceed those found here during fast-starts.

The range of comparative data now available on *in vivo* patterns of bone deformation in

vertebrates during normal functional activity permits the following conclusions about vertebrate bone and normal loading patterns. (1) Vertebrate bone is rarely subjected to strain rates higher than $100\times10^3\,\mu\varepsilon/s$. Only during extremely rapid movements (such as fast-start acceleration or suction feeding in fishes) do strain rates rise above this value. (2) Vertebrate bone is rarely subjected to strain magnitudes greater than $3100\,\mu\varepsilon$. These peak values have only been recorded during fast locomotion in horses and fast-start accelerations in fishes. (3) Vertebrate bone is rarely subjected to pure bending or pure axial tensile or compressive stresses. Some degree of torsional stress has been found in nearly all *in vivo* analyses of bone deformation. (4) Bone mass appears to be adjusted to regulate the strain level to which it is subjected during normal functional activity. The sunfish operculum and the horse radius, bones which differ in mass by a factor of at least 10^2, both are subjected to peak strain magnitudes of over $3000\,\mu\varepsilon$. During steady locomotion, both the rat femur and the sunfish hypural undergo similar deformations (500–$1000\,\mu\varepsilon$; 10–$20\times10^3\,\mu\varepsilon/s$).

Prospectus

While this study has provided additional comparative data on vertebrate bone deformation patterns and has aided in defining the range of strain values and rates that vertebrate bone is subjected to *in vivo*, it only serves as an initial indication of structure/function relationships in the tail of ray-finned fishes. Given the importance of external and internal structural changes in caudal morphology for the study of actinopterygian evolution (Affleck, 1950; Nursall, 1956, 1962; Alexander, 1967; Rosen, 1973; Webb, 1982), a number of important questions remain to be examined in a comparative study of locomotor morphology and bone strain patterns. (1) Do externally asymmetrical tails subject the hypurals to different patterns of stress and strain than externally symmetrical tails? (2) Is the alignment of the principal stresses perpendicular to and parallel to the body axis during fast-starts a general phenomenon? (3) Is the difference in orientation of principal strain axes between fast-starts and continuous locomotion common to many teleost fishes and if so, does this difference relate to morphological and functional compromises identified by Webb (1978, 1982) for steady versus unsteady locomotion? (4) What is the role of the intrinsic caudal musculature during fast-starts and steady swimming, and is muscle activity capable of modifying the stresses seen by the skeletal elements? These questions relate directly to the relationship between externally imposed loads and internal structural patterns in the skeleton and musculature, an area of fish locomotion that will need to receive increasing attention as the study of actinopterygian locomotor patterns progresses.

I thank the Society of Fellows, Harvard University and the Penrose fund of the American Philosophical Society for support of this research, and Bill and Sara Fink for discussions of caudal anatomy. I am grateful to those who provided unpublished data for the comparative analysis of strain rates and magnitudes: W. Hylander, A. Biewener, L. Lanyon, and C. Rubin. Finally, special thanks go to Dr L. Lanyon for his help in performing many of the experiments and for advice and comments on the manuscript. Dr Paul Webb also made many valuable suggestions and comments on the manuscript.

REFERENCES

Affleck, R. J. (1950). Some points in the function, development, and evolution of the tail in fishes. *Proc. zool. Soc. Lond.* **120**: 349–368.

Alexander, R. McN. (1967). *Functional design in fishes*. London: Hutchinson and Co.

Bainbridge, R. (1958). The speed of swimming fish as related to size and to the frequency and the amplitude of the tail beat. *J. exp. Biol.* **35**: 109–133.
Bainbridge, R. (1963). Caudal fin and body movements in the propulsion of some fish. *J. exp. Biol.* **40**: 23–56.
Blake, R. W. (1979). The energetics of hovering in the mandarin fish (*Synchropus picturatus*). *J. exp. Biol.* **82**: 25–33.
Cowan, G. I. (1969). The cephalic and caudal musculature of the sculpin *Myoxocephalus polyacanthocephalus* (Pisces: Cottidae). *Can. J. Zool.* **47**: 841–850.
Eaton, R. C., Bombardieri, R. A. & Meyer, D. L. (1977). The mauthner-initiated startle response in teleost fish. *J. exp. Biol.* **66**: 65–81.
Fierstine, H. L. & Walters, V. (1968). Studies in locomotion and anatomy of scombroid fishes. *Mem. S. Calif. Acad. Sci.* **6**: 1–31.
Gero, D. R. (1952). The hydrodynamic aspects of fish propulsion. *Am. Mus. Nov.* No. 1601: 1–32.
Hoar, W. S. & Randall, D. J. (1978). *Fish physiology* **7**. New York: Academic Press.
Hylander, W. L. (1979). Mandibular function in *Galago crassicaudatus* and *Macaca fascicularis*: an *in vivo* approach to stress analysis of the mandible. *J. Morph.* **159**: 253–296.
Lanyon, L. E. (1973). The analysis of surface bone strain in the calcaneus of sheep during normal locomotion. *J. Biomech.* **6**: 41–49.
Lanyon, L. E. (1976). The measurement of bone strain *in vivo*. *Acta Orthop. Belg.* **42** (Suppl. 1): 98–108.
Lanyon, L. E. & Rubin, C. T. (1980). Loading of mammalian long bones during locomotion. *J. Physiol.* **303**: 72.
Lauder, G. V. (1980). On the relationship of the myotome to the axial skeleton in vertebrate evolution. *Paleobiol.* **6**: 51–56.
Lauder, G. V. & Lanyon, L. E. (1980). Functional anatomy of feeding in the bluegill sunfish, *Lepomis macrochirus*: *in vivo* measurement of bone strain. *J. exp. Biol.* **84**: 33–55.
Lighthill, J. (1975). *Mathematical biofluiddynamics*. Philadelphia, Pennsylvania: Soc. Indust. Appl. Math.
Nag, A. C. (1967). Functional morphology of the caudal region of certain clupeiform and perciform fishes with reference to the taxonomy. *J. Morph.* **123**: 529–558.
Nursall, J. R. (1956). The lateral musculature and the swimming of fish. *Proc. zool. Soc. Lond.* **126**: 127–143.
Nursall, J. R. (1962). Swimming and the origin of paired appendages. *Am. Zool.* **2**: 27–41.
Nursall, J. R. (1963). The caudal musculature of *Haplopagrus guntheri* Gill (Perciformes, Lutjanidae). *Can. J. Zool.* **41**: 865–880.
Patterson, C. (1968*a*). The caudal skeleton in Lower Liassic pholidophorid fishes. *Bull. Br. Mus. nat. Hist. (Geol.)* **16**: 201–239.
Patterson, C. (1968*b*). The caudal skeleton in Mesozoic acanthopterygian fishes. *Bull. Br. Mus. nat. Hist. (Geol.)* **17**: 47–102.
Patterson, C. (1973). Interrelationships of holosteans. In *Interrelationships of fishes*: 233–305. Greenwood, P. H., Miles, R. S. and Patterson, C. (Eds). London: Academic Press.
Patterson, C. & Rosen, D. E. (1977). Review of ichthyodectiform and other Mesozoic teleost fishes and the theory and practice of classifying fossils. *Bull. Am. Mus. nat. Hist.* **158**: 81–171.
Rosen, D. E. (1973). Interrelationships of higher euteleostean fishes. In *Interrelationships of fishes*: 397–513. Greenwood, P. H., Miles, R. S. and Patterson, C. (Eds). London: Academic Press.
Schaeffer, B. (1967). Osteichthyan vertebrae. *J. Linn. Soc. Lond.* **47**: 185–195.
Videler, J. J. (1975). On the interrelationships between morphology and movement in the tail of the cichlid fish *Tilapia nilotica* (L.). *Neth. J. Zool.* **25**: 143–194.
Videler, J. J. (1977). Mechanical aspects of fish tail joints. *Fortschr. Zool.* **24**: 183–194.
Webb, P. W. (1975). Hydrodynamics and energetics of fish propulsion. *Bull. Fish. Res. Bd Can.* **190**: 1–158.
Webb, P. W. (1977). Effects of median fin amputation on fast-start performance of rainbow trout (*Salmo gairdneri*). *J. exp. Biol.* **68**: 123–135.
Webb, P. W. (1978). Fast-start performance and body form in seven species of teleost fish. *J. exp. Biol.* **74**: 211–226.
Webb, P. W. (1982). Locomotor patterns in the evolution of actinopterygian fishes. *Am. Zool.* **22** (2).
Weihs, D. (1972). A hydrodynamic analysis of fish turning manoeuvres. *Proc. R. Soc. Lond.* (B) **182**: 59–72.
Weihs, D. (1973). The mechanism of rapid starting of slender fish. *Biorrhology* **10**: 343–350.
Winterbottom, R. (1974). A descriptive synonymy of the striated muscles of the Teleostei. *Proc. Acad. nat. Sci. Phil.* **125**: 225–317.
Wu, T. Y. (1971). Hydromechanics of swimming propulsion. Part I. Swimming of a two-dimensional flexible plate at variable forward speeds in an inviscid fluid. *J. Fluid Mech.* **46**: 337–355.